Mean and Flux Horizontal Variability of Virtual Potential Temperature, Moisture, and Carbon Dioxide: Aircraft Observations and LES Study

MONICA GÓRSKA AND JORDI VILÀ-GUERAU DE ARELLANO

Meteorology and Air Quality Section, Wageningen University, Netherlands

MARGARET A. LEMONE

National Center for Atmospheric Research, Boulder, Colorado

CHIEL C. VAN HEERWAARDEN

Meteorology and Air Quality Section, Wageningen University, Netherlands

(Manuscript received 19 April 2007, in final form 26 March 2008)

ABSTRACT

The effects of the horizontal variability of surface properties on the turbulent fluxes of virtual potential temperature, moisture, and carbon dioxide are investigated by combining aircraft observations with large-eddy simulations (LESs). Daytime fair-weather aircraft measurements from the 2002 International H_2O Project's 45-km Eastern Track over mixed grassland and winter wheat in southeast Kansas reveal that the western part of the atmospheric boundary layer was warmer and drier than the eastern part, with higher values of carbon dioxide to the east. The temperature and specific humidity patterns are consistent with the pattern of surface fluxes produced by the High-Resolution Land Data Assimilation System. However, the observed turbulent fluxes of virtual potential temperature, moisture, and carbon dioxide, computed as a function of longitude along the flight track, do not show a clear east–west trend. Rather, the fluxes at 70 m above ground level related better to the surface variability quantified in terms of the normalized differential vegetation index (NDVI), with strong correlation between carbon dioxide fluxes and NDVI.

A first attempt is made to estimate the ratios of the flux at the entrainment zone to the surface flux (entrainment ratios) as a function of longitude. The entrainment ratios averaged from these observations ($\beta_{\theta_v} \approx 0.10$, $\beta_q \approx -2.4$, and $\beta_{CO_2} \approx -0.58$) are similar to the values found from the homogeneous LES experiment with initial and boundary conditions similar to observations.

To understand how surface flux heterogeneity influences turbulent fluxes higher up, a heterogeneous LES experiment is performed in a domain with higher sensible and lower latent heat fluxes in the western half compared to the eastern half. In contrast to the aircraft measurements, the LES turbulent fluxes show a difference in magnitude between the eastern and western halves at 70 and 700 m above ground level. Possible reasons for these differences between results from LES and aircraft measurements are discussed.

1. Introduction

Previous studies of the diurnal variability of carbon dioxide (CO_2) focus mainly on surface processes such as photosynthesis and respiration (Verma et al. 1989; Kim and Verma 1990; Lloyd and Taylor 1994), rather than on the CO_2 exchange between the atmospheric boundary layer (ABL) and the free atmosphere during daytime. This last process is driven by energy generated within the boundary layer, primarily by buoyancy, and shear at the ABL top. Vilà-Guerau de Arellano et al. (2004) studied this process by combining aircraft and surface observations with mixed-layer modeling. They studied the influence of the boundary layer evolution on CO_2 diurnal variability, focusing in particular on CO_2 exchange at the interface and its relation to the boundary layer evolution. Entrainment of air with low CO_2 mixing ratios appeared to dominate CO_2 evolution in the morning hours, associated with the rapid growth of the ABL. However, in the afternoon the CO_2 uptake by the grass vegetation became the dominant factor in the CO_2 diurnal variability.

The majority of the ABL studies concerned with the

Corresponding author address: Jordi Vilà-Guerau de Arellano, Meteorology and Air Quality Section, Droevendaalsesteeg 4, Atlasgebouw, 6700 AA Wageningen, Netherlands.
E-mail: jordi.vila@wur.nl

DOI: 10.1175/2008MWR2230.1

vertical structure of the turbulent fluxes and entrainment assume a homogeneous surface. However, the land surface can be rather heterogeneous, resulting in horizontal variability in the surface fluxes. The entrainment of heat, moisture, and carbon dioxide could be influenced by the variability of the surface properties as well. Analysis of idealized large-eddy simulations has shown that the interface between the ABL and the free atmosphere is influenced by processes related to land surface heterogeneity (Avissar and Schmidt 1998; Patton et al. 2005). Concerning entrainment at the inversion layer and the boundary layer growth, there is still not a clear quantification of whether entrainment is enhanced by the heterogeneity of the underlying land surface (Avissar and Schmidt 1998) or if it is similar to entrainment above homogeneous surfaces (Patton et al. 2005). Closely related to these variations, several studies have attempted to determine the heterogeneity effect on the boundary layer structure by proposing several heterogeneity length scales (Mahrt 2000; Patton et al. 2005; Strunin and Hiyama 2005). Mahrt (2000) found the strongest effects on the ABL properties if the heterogeneity length scale is between 2 and 20 km. Kang et al. (2007) calculated the minimum heterogeneity length scale that influences the flow through the whole ABL for 5 days at the north–south track in the 2002 International H_2O Project (IHOP_2002). They estimated values of a few kilometers, except for one particular day when the length scale was one order of magnitude smaller than on the other days.

The influence of surface heterogeneity on the horizontal variability of the turbulent fluxes is also discussed by Kang et al. (2007) and LeMone et al. (2003, 2007a,b). While Kang et al. (2007) studied heterogeneity related to soil moisture, LeMone et al. (2007a) related horizontal flux gradients to vegetation. From analyzing two field projects, the Cooperative Atmospheric Surface Exchange Study 1997 (CASES-97) and IHOP_2002, LeMone et al. (2007a) found that land-use patterns have a strong influence on the horizontal distribution of sensible heat (H) and latent heat (LE) fluxes. The dominant vegetation types, grass and winter wheat, reverse roles with the season: while the grass was green and the winter wheat was senescent in IHOP_2002 (summer), the winter wheat was growing and the grass was dormant in CASES-97 (spring). Therefore, H minima (maxima) in IHOP_2002 correspond to H maxima (minima) in CASES-97. For the latent heat fluxes, the correspondence was less clear.

Our research extends the previous studies to examine the effect of the horizontal variability of surface properties on the vertical flux profiles of virtual potential temperature, moisture, and CO_2. The study is mainly focused on the sensitivity of the convective boundary layer evolution and the fluxes at the entrainment zone to changes in land surface characteristics. Surface and aircraft measurements of the thermodynamic variables and CO_2 from IHOP_2002 (LeMone et al. 2007b,a; Weckwerth et al. 2004) are analyzed and combined with large-eddy simulation experiments. Due to variations in land surface properties, large horizontal variability in H and LE in the vicinity of the flight track was predicted by a land surface model. This variability has the potential to influence the boundary layer dynamics and entrainment. Therefore, the main goals of this research are 1) estimating the means of virtual potential temperature, moisture, and CO_2 and their turbulent fluxes as a function of height and longitude using aircraft measurements and large-eddy simulations; 2) relating the horizontal variability of the turbulent fluxes to the horizontal variability of the surface properties; and 3) estimating the entrainment ratios for virtual potential temperature, moisture, and CO_2 as a function of longitude and discussing their variability.

The observations, the large-eddy simulation model, and the methods used to calculate the turbulent fluxes are explained in section 2. In section 3, the observations and simulations of the vertical and horizontal structure of the thermodynamic variables, CO_2, and its turbulent fluxes are discussed. Finally, our conclusions are presented in the last section.

2. Method

a. Observations

Surface and aircraft data were gathered during IHOP_2002, which took place over the U.S. southern Great Plains in May and June 2002. The aim of IHOP_2002 was to realize gains in the prediction of convective precipitation in numerical weather prediction models by improving the water vapor measurements and the representation of the water vapor evolution. An overview of this project and documentation of its instruments can be found in Weckwerth et al. (2004).

Within the framework of IHOP_2002, LeMone et al. (2007a) studied the influence of horizontal variability in vegetation and soil moisture on the horizontal distribution of sensible and latent heat fluxes. By analyzing the aircraft measurements, we extend their study by calculating the vertical structure of the turbulent fluxes of virtual potential temperature, specific humidity, and CO_2, as well as the horizontal variability of the CO_2 fluxes.

We have selected 30 May 2002 because it has favorable conditions for calculating turbulent fluxes at dif-

TABLE 1. Main characteristics and average values of the 16 horizontal aircraft legs at different mean heights $\bar{z}$.

Leg	Time (CST)	$\bar{z}$ (m AGL)	$\overline{\theta_v}$ (K)	$\overline{q}$ (g kg^{-1})	$\overline{CO_2}$ (ppm)	$\overline{w'\theta_v'}$ (K m s^{-1})	$\overline{w'q'}$ (g kg^{-1} m s^{-1})	$\overline{w'CO_2'}$ (ppm m s^{-1})
1	1044:04–1052:08	837*	304.8	5.23	367.4	−0.008	0.02	−0.02
2	1054:04–1103:36	68	301.6	13.29	359.7	0.087	0.10	−0.34
3	1105:11–1114:50	61	301.8	13.29	359.6	0.099	0.14	−0.25
4	1117:20–1126:21	523	302.0	12.85	359.5	0.032	0.19	−0.29
5	1128:25–1138:03	62	302.1	13.22	358.0	0.094	0.11	−0.35
6	1139:54–1149:38	66	302.2	13.15	357.9	0.085	0.12	−0.24
7	1153:59–1203:19	525	302.4	12.95	358.5	0.056	0.21	−0.18
8	1204:55–1214:57	73	302.5	13.01	358.3	0.106	0.17	−0.24
9	1216:40–1226:05	599	302.7	12.77	358.5	0.033	0.20	−0.22
10	1229:29–1239:08	65	302.7	13.09	358.5	0.099	0.12	−0.28
11	1241:19–1250:34	690	303.0	12.57	358.9	0.041	0.29	−0.20
12	1252:43–1302:09	71	303.0	13.05	357.8	0.129	0.18	−0.46
13	1305:49–1314:37	679	303.2	12.86	357.5	0.069	0.22	−0.33
14	1316:17–1326:14	71	303.3	12.94	356.9	0.116	0.20	−0.38
15	1329:20–1338:40	1357*	307.2	6.34	363.9	0.004	−0.07	0.10
16	1341:29–1351:06	689	303.5	12.58	356.4	0.031	0.19	−0.19

* Above the ABL.

ferent heights. The boundary layer developed as a typical well-mixed boundary layer, which grew steadily from 600 m at 1000 central standard time (CST) to 1100 m at 1400 CST. The meteorological conditions were characterized by clear skies and a steady southeast wind of 4 m s^{-1}. The aircraft (University of Wyoming King Air) flew above a site vegetated with mostly grass and with more winter wheat in the west—with soil moisture increasing eastward. Thus, some horizontal variability in the turbulent fluxes could be expected.

The aircraft flew 8 vertical soundings and 16 horizontal legs along a fixed flight track [the IHOP_2002 "Eastern Track"; shown in Fig. 1 of LeMone et al. (2007b)] southeast of Beaumont, Kansas, between 1100 and 1400 CST. The lengths of the horizontal legs are approximately 45 km. Eight horizontal legs were flown at around 70 m above ground level (AGL), six legs higher in the boundary layer between 500 and 700 m AGL and two legs in the free atmosphere. The main characteristics and average values of the 16 horizontal aircraft legs are given in Table 1. The sampling frequency of the sensors is 25 Hz, corresponding to one sample each 3 m.

Figure 1 shows the surface sensible and latent heat flux values in the vicinity of the aircraft track at 1300 CST based on land surface model runs using the High-Resolution Land Data Assimilation System (HRLDAS; Chen et al. 2007). The top panel in Fig. 1 indicates large heterogeneity in the area, with larger sensible heat fluxes in the west (250–350 W m^{-2}) than in the east (200–300 W m^{-2}). In contrast, the latent heat fluxes (bottom panel in Fig. 1) are higher at the eastern part: Values range between 300–400 W m^{-2} (west) and 350–450 W m^{-2} (east). Values for volumetric soil moisture (not shown) are between 0.23–0.25 (west) and 0.25–0.27 (east). The eastward decrease in the Bowen ratio (from 0.9 in the west to 0.6 in the east) is consistent with the climatology of the region.

Turbulent fluxes of virtual potential temperature, moisture, and CO_2 are calculated using two methods: (a) a method in which one single flux value is obtained for each leg (referred to as the single-value method) and (b) a method in which the fluxes are calculated as a function of longitude along the flight track (referred to as the horizontal variability method). The single-value approach of calculating the fluxes is as follows: 1) linearly detrend the quantities w (= vertical velocity) and ψ (= potential temperature θ, moisture q, or carbon dioxide concentration CO_2) to acquire w' and ψ' using $w' = w - \overline{w}$ and $\psi' = \psi - \overline{\psi}$, 2) correlate the quantities w' and ψ' to obtain $w'\psi'$, and 3) average $w'\psi'$ over the total leg to obtain one value, $\overline{w'\psi'}$, for each leg.

To study the effects of surface heterogeneity on the magnitude of the fluxes, fluxes should be calculated as a function of the distance along the flight track (approximately along the longitude in our measurement dataset). Reliable estimates of the horizontal variation of the turbulent fluxes are needed in order to minimize the statistical uncertainty. Longitude-dependent turbulent fluxes are calculated following the method proposed by LeMone et al. (2003). Briefly, it consists of the following steps: 1) linearly detrending the quantities w and ψ over the total leg, 2) correlating the quantities w' and ψ', 3) averaging $w'\psi'$ over 0.01° longitude segments (approximately 1 km; 300-point measurements) to obtain values for $\overline{w'\psi'}$, and 4) smoothing by taking a 4-point (≈4 km) running average to obtain longitude-dependent values, $\overline{w'\psi'}$. An important property of this method is that the average of the one-point longitude-

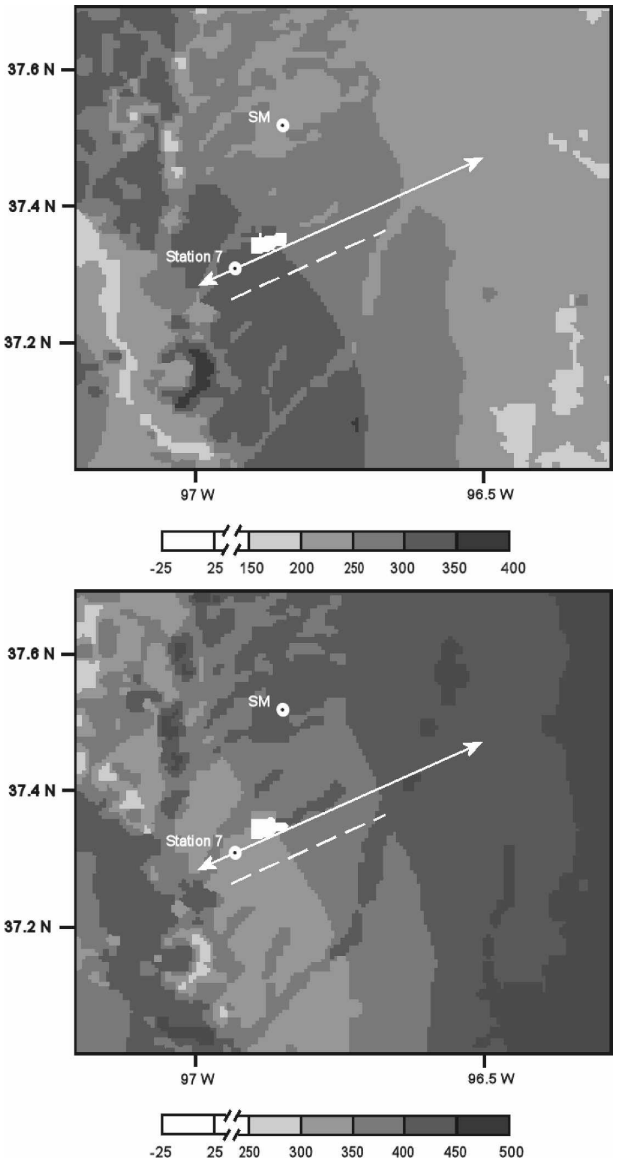

FIG. 1. (top) Sensible heat fluxes and (bottom) latent heat fluxes (W m^{-2}) at the surface in the vicinity of the 45-km aircraft track (white arrow: 37.30°N, 96.96°W–37.47°N, 96.51°W) at 1300 CST. The fluxes are calculated by combining a land surface model run from HRLDAS with satellite observations from the Moderate Resolution Imaging Spectraradiometer (MODIS) on 30 May 2002. The white area is the Timber Creek Lake. The heterogeneous LES "track" (dotted line) and two surface stations [station 7 and the Smileyberg site (SM)] are also shown.

dependent fluxes over the total flight length corresponds to the average flux calculated from the single-value method.

Although these two methods are applied in the next section, other techniques for calculating the turbulent fluxes are applied to the data and compared to our two methods. In particular, three different detrending techniques are compared: linear detrending over the total flight leg, linear detrending over half the flight leg, and detrending by 1-km averages. Subtracting averages over smaller parts is similar to the method used by Mahrt et al. (1994). The spatial variation of the sensible and latent heat fluxes is similar for all three detrending techniques, although the mean heat flux over the total horizontal leg is sensitive to the technique that is used. If the averaging is performed over a shorter length, the calculated heat flux becomes smaller. Linear detrending over the total flight leg is chosen because a longer averaging process is able to incorporate the contribution of the larger eddies to the fluxes.

To study the sensitivity of the fluxes to the number of points in the running average, the fluxes are calculated by applying three different averages: one-point averaging (original curve), two-point running averaging, and four-point running averaging. As shown in LeMone et al. (2003), the smaller-scale variations are filtered out and, consequently, the flux pattern gets smoother when using a larger number of points in the running mean. Although the horizontal variability is reduced, the statistical confidence increases, as shown in their Fig. 10. In this study, the four-point (≈4 km) averaging is chosen in our horizontal variability method, since it shows the large-scale variability of the fluxes with an acceptable uncertainty.

A relevant aspect in using the horizontal variability method is the ability to study the correlations between the surface characteristics and the turbulent fluxes at different heights. The variability of the surface properties is quantified in terms of the normalized differential vegetation index (NDVI), which represents the proportion of photosynthetic activity. NDVI is measured by the aircraft using reflectance from the red (ρ_{red}) and near-infrared (ρ_{nIR}) wave bands and is defined as

$$\mathrm{NDVI} = \frac{\rho_{nIR} - \rho_{red}}{\rho_{nIR} + \rho_{red}}. \quad (1)$$

The aircraft measurements were supplemented with surface observations of sensible and latent heat fluxes at one surface station (station 7) along the aircraft track. Argonne National Laboratory operated another surface flux site close to the track, a grass site at Smileyberg, Kansas, which measured CO_2 fluxes (Coulter et al. 2006). These measurements from station 7 and the Smileyberg site are used for comparison with the surface fluxes in the analysis of the single-value method and as an input surface forcing in the numerical experiments (Fig. 2).

b. Large-eddy simulation model

To support the observational study, a large-eddy simulation (LES) model is used to study the evolution

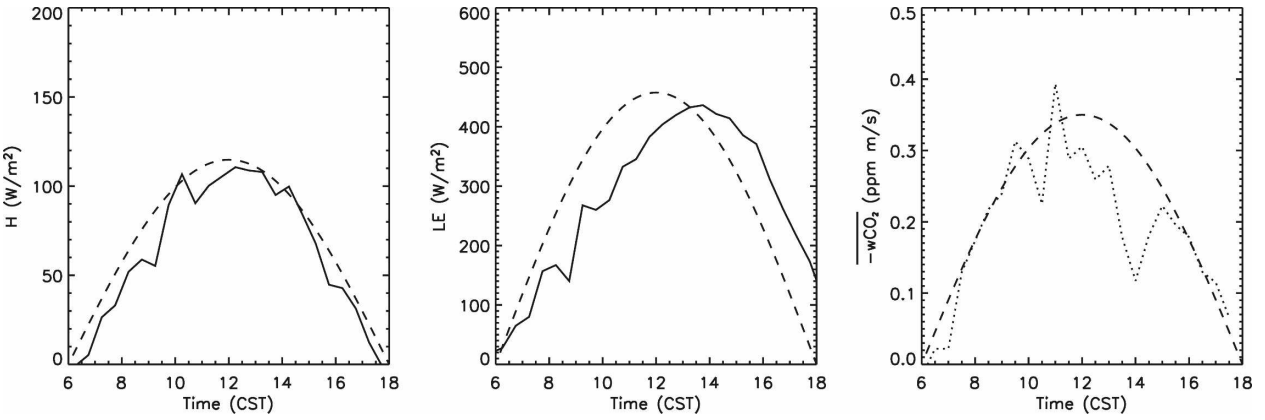

FIG. 2. (left) Sensible heat, (middle) latent heat, and (right) carbon dioxide surface flux evolution. The surface fluxes prescribed in the LES numerical experiment are indicated by the dashed line. The observed surface sensible and latent heat flux at station 7 (37.31°N, 96.93°W) are plotted with the continuous line. The measured carbon dioxide flux at the Smileyberg site (37.52°N, 96.85°W) is shown with a dotted line.

of the vertical structure of the turbulent fluxes. The goal of the simulation is to obtain additional and supporting information on the diurnal development of the boundary layer on 30 May 2002. In addition, the evolution of the vertical mean and flux profiles from the early morning to late afternoon can be explicitly calculated and compared to the aircraft measurements. Two numerical experiments are carried out: one experiment with homogeneous surface fluxes and one experiment with heterogeneous surface fluxes maintaining the same available energy, H + LE, over the two domains.

The LES solves the Navier–Stokes equations explicitly for the motions larger than the filter size. For motions smaller than the filter size, the so-called subgrid-scale (SGS) components are represented as a function of the resolved variables. These SGS components are calculated by using a TKE closure scheme (Deardorff 1980). The lateral conditions are cyclic and there is a no-slip boundary condition at the surface. More details about this model can be found in Cuijpers and Duynkerke (1993) and Siebesma and Cuijpers (1995). We used the recently developed parallel version, which is extensively described in Dosio et al. (2003).

In this study, the space and time integrations for the advection terms of temperature and scalars are computed with a fifth-order advection and a third-order Runge–Kutta numerical scheme, respectively (Wicker and Skamarock 2002). The considered domain is 25.6 × 25.6 × 2.7 km^3 with a grid length of 100 m for the horizontal directions and 25 m for the vertical direction. Consequently, the LES domain is discretized in 256 × 256 × 108 grid cells. By using this large domain, the horizontal dimension of the model is about 60% of the flight track length. The model simulation was run for 12 h from 0600 to 1800 CST.

Our motivation is to design numerical experiments with surface forcings similar to the ones observed on 30 May 2002. In the homogeneous experiment, the surface fluxes are sinusoidal functions of time based on the measured values at surface station 7 and the Smileyberg site (Fig. 2). Furthermore, the initial vertical profiles of the potential temperature, specific humidity, and CO_2 mixing ratio at 0600 CST are chosen such that the vertical LES profiles at 1200 and 1300 CST closely fit the vertical sounding observations at the west end of the track at 1200 and 1300 CST (Fig. 3). The prescribed initial mixed layer values, jump values at the inversion layer, initial boundary layer height, and surface fluxes at 0600 CST are also given in Table 2. Due to low wind velocities on this day (4 m s^{-1}), we have assumed u = v = 0 for simplicity (Table 2).

The heterogeneous case is defined by prescribing different amplitudes in the surface fluxes for the east and west halves of the domain such that the available energy, H + LE = R_{net} − G, is constant for both domains and similar to the homogeneous experiment. In the western half of the domain, the sensible heat fluxes are prescribed 20% higher and the latent heat fluxes 5% lower than the homogeneous case. In the eastern half, the sensible heat fluxes are prescribed 20% lower and the latent heat fluxes 5% higher than the homogeneous case. The carbon dioxide fluxes were not changed for the heterogeneous case. This experiment provides a way to quantify if the surface flux heterogeneity has an effect on the horizontal fluxes higher in the boundary layer and the boundary layer height evolution.

To calculate the turbulent fluxes for the homogeneous case, the variables are averaged in space over a horizontal plane and averaged in time over 15 min, a little larger than the time required for the King Air to

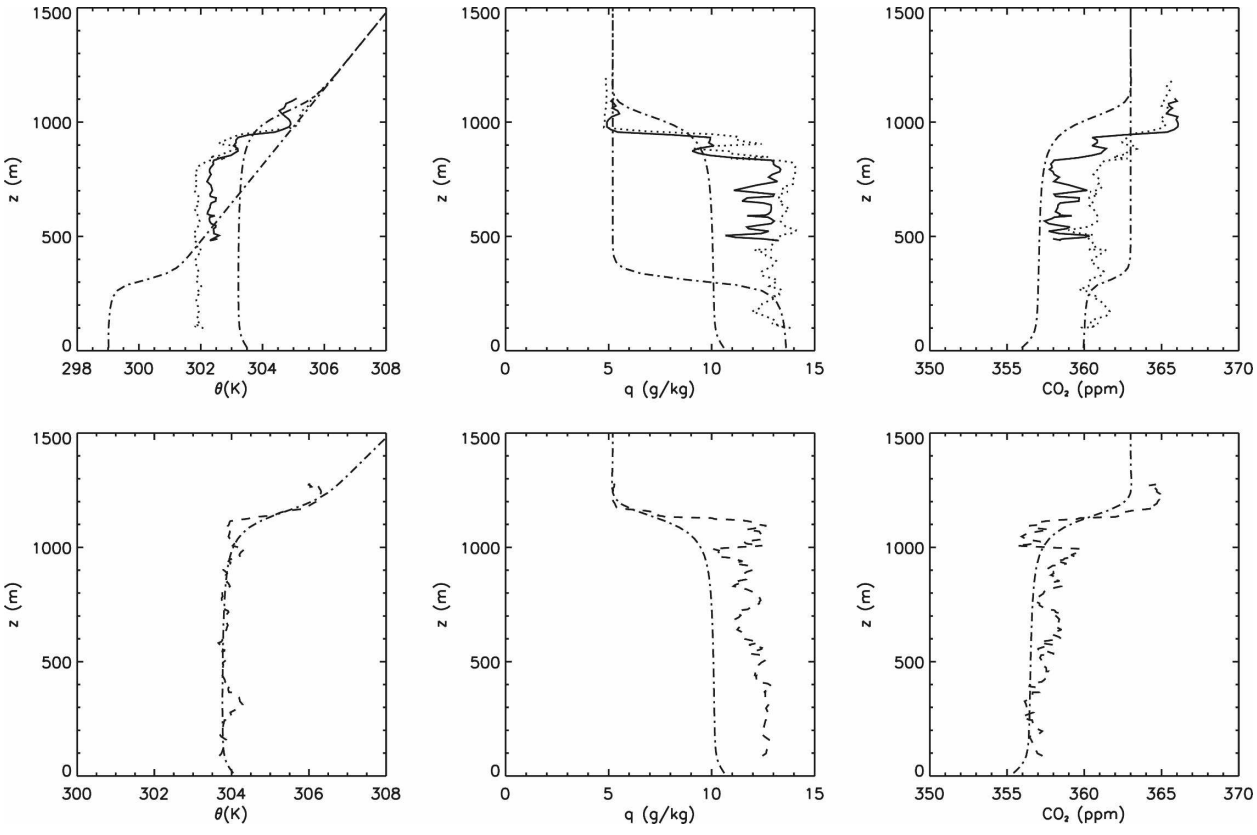

FIG. 3. LES (dashed–dotted line) vertical profiles for (left) potential temperature, (middle) specific humidity, and (right) carbon dioxide mixing ratio from the homogeneous LES experiment at 0600 CST and at (top) 1200 and (bottom) 1300 CST. Observed vertical profiles from vertical soundings at 1152 CST West (solid line), at 1227 CST East (dotted line), and at 1302 CST West (dashed line). A potential temperature jump of 2 K, a specific humidity jump of -7 g kg^{-1}, and a CO_2 jump of -7 ppm is observed for the two west soundings. No vertical aircraft soundings are available at 0600 CST.

fly one leg. Notice that the method used to calculate the fluxes is similar to the single-value method, but the main difference in calculating the fluxes between the homogeneous LES experiment and the aircraft observations is the spatial averaging over a 25.6×25.6 km^2 area (LES) versus a 45-km horizontal track (observations). For the heterogeneous case, the method used to calculate the fluxes is more similar to the horizontal variability method, but the variables are averaged first over the homogeneous north–south direction. After that, the data are detrended over the 25.6 km, correlated and averaged over 1-km segments in the west–east direction.

3. Results and discussion

First, the boundary layer structure is analyzed with the single-value method, which calculates one single flux value for each horizontal aircraft leg. This value represents the total length below the aircraft leg. Second, possible differences between the west and east parts of the track that are due to variations in land surface properties are discussed. In studying the flux variability, mean quantities and fluxes are calculated accounting for their possible variation due to changes in the surface properties.

a. Vertical structure

Vertical soundings were flown at both ends of the track between 1100 and 1400 CST. Figure 3 shows vertical profiles for potential temperature, virtual potential temperature, specific humidity, and CO_2 mixing ratio at the western and eastern parts of the track. Figure 3 also shows a well-mixed boundary layer, and the boundary layer (BL) at the west end of the track grows from 800 m at 1152 CST to 1100 m at 1302 CST. During this period, the potential temperature in the BL increases from 302 to 304 K with an almost constant potential temperature jump of 2 K at the inversion layer. The two specific humidity profiles are quite similar and show constant values between 12 and 13 g kg^{-1} in the BL and constant jumps of -7 g kg^{-1} between the BL and the

TABLE 2. The prescribed initial mixed-layer values, jump values at the inversion layer, initial boundary layer height, and surface fluxes at 0600 CST used to initiate the homogeneous LES simulation [t = time (h) and T = 12 h]. These values are based on the surface measurements and indirectly on the aircraft profile measurements.

θ_0	299 K
$\Delta\theta_0$	2 K
γ_θ	$6\ 10^{-3}$ K m^{-1}
q_0	13.6 g kg^{-1}
Δq_0	−8.4 g kg^{-1}
CO_{2_0}	360 ppm
ΔCO_{2_0}	3 ppm
u_0, v_0	0 m s^{-1}
Δu_0, Δv_0	0 m s^{-1}
z_0	300 m
$\overline{(w'\theta')_0}$	$0.10 \sin[\pi(t-6)/T]$ K m s^{-1}
$\overline{(w'q')_0}$	$0.16 \sin[\pi(t-6)/T]$ g kg^{-1} m s^{-1}
$\overline{(w'CO_2')_0}$	$-0.35 \sin[\pi(t-6)/T]$ ppm m s^{-1}

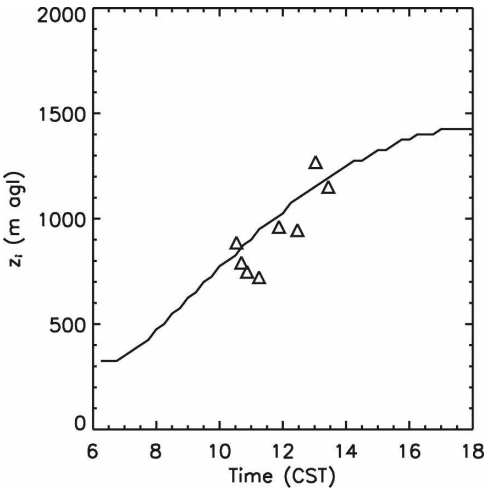

FIG. 4. The boundary layer height evolution calculated with the maximum potential temperature gradient from the homogeneous LES experiment (solid line) and from the vertical aircraft soundings (symbols).

free atmosphere. The CO_2 mixing ratio in the BL also remains quite constant in time at 358 ppm with a positive CO_2 jump of nearly 7 ppm at the western end of the track. Due to this positive CO_2 jump, downward CO_2 transport (negative CO_2 flux) is expected from the free atmosphere.

Focusing on carbon dioxide, these results are similar to those of many other studies. Yi et al. (2004) and Gerbig et al. (2003) also showed positive CO_2 jumps at the top of the boundary layer from aircraft measurements. In addition, Desjardins et al. (1992) calculated negative CO_2 fluxes at the inversion layer from aircraft measurements, which also indicate a positive CO_2 jump. However, Vilà-Guerau de Arellano et al. (2004) estimated large positive CO_2 fluxes. In their study, the CO_2 mixing ratio was higher in the BL (392 ppm) than in the free atmosphere (362 ppm) at 0816 UTC in the morning due to the release of CO_2 at night, before convective turbulence starts to develop. This is consistent with the observed negative CO_2 jump at the inversion layer (−30 ppm) and upward CO_2 transport during the morning hours when the ABL was growing rapidly.

Table 1 shows the leg-averaged (single value method) fluxes of virtual potential temperature, specific humidity and CO_2 for the 16 horizontal legs between 1100 and 1400 CST. The flux values at 70 m show certain variability ($\overline{w'\theta_v'} = 0.085 - 0.13$ K m s^{-1}, $\overline{w'q'} =$ 0.10–0.20 g kg^{-1} m s^{-1} and $\overline{w'CO_2'} = -0.25 - -0.45$ ppm m s^{-1}). In spite of this variability, these values are in close agreement to the ones measured at the surface stations between 1100 and 1400 CST (Fig. 2). The fluxes are consistent with typical behavior, with heat and moisture transported upward from the surface into the BL and carbon dioxide is transported downward from the BL to the surface, consistent with net uptake of CO_2 (photosynthesis larger than respiration) by the green vegetation at the surface.

Using surface flux values comparable to those of surface station 7 and the Smileyberg site (Fig. 2), and using initial conditions of the thermodynamic variables and CO_2 at 0600 CST (Table 2) such that the LES profiles at 1200 and 1300 CST fit the observed vertical west profiles at these times on 30 May 2002 (Fig. 3), the daily evolution of the boundary layer is simulated with a large-eddy simulation model. By doing so, we are able to obtain continuous calculations of the vertical profiles of the mean variables and fluxes, as well as the ABL evolution. The ABL depth values are crucial for extrapolating the aircraft measurements to the top of the boundary layer in order to estimate the entrainment fluxes.

Figure 4 shows the evolution of the ABL depth based on the homogeneous LES experiment and the vertical aircraft soundings. The ABL depth (z_i) is determined by the maximum potential temperature gradient (Sullivan et al. 1998). The vertical potential temperature profiles measured by the aircraft are smoothed to be able to calculate the maximum gradient. Although some variability exists, the agreement is reasonable between the aircraft observations and the model calculations. Thus, the ABL depth calculated from the LES is used as a scaling parameter for both the aircraft and LES entrainment flux estimates. In spite of the spatial gradient of the ABL depth, which is 100–200 m along the flight track (not shown), we have assumed a constant ABL depth along the flight track for simplicity.

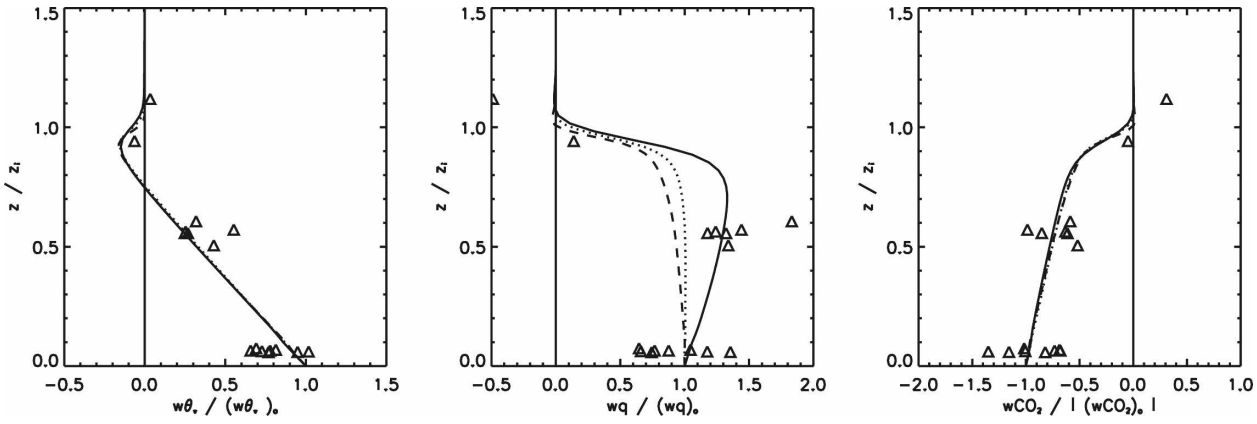

FIG. 5. Vertical profiles of (left) dimensionless buoyancy flux, (middle) specific humidity flux, and (right) carbon dioxide flux for 1000 (solid line), 1200 (dotted line), and 1400 CST (dashed line) calculated from the homogeneous LES experiment. Symbols represent the aircraft measurements between 1100 and 1400 CST. Scaling is performed with the surface fluxes (Table 2) and the boundary layer heights determined by the maximum potential temperature gradient from the calculated vertical temperature profiles using the homogeneous LES experiment. Notice that the (left) buoyancy and (right) carbon dioxide flux profiles are clustered around a single curve due to the scaling presentation.

This 100–200-m uncertainty in ABL depth estimates is addressed in section 3b.

The dimensionless vertical profiles of the buoyancy, moisture, and carbon dioxide fluxes calculated from the homogeneous LES data and the aircraft observations are shown in Fig. 5. The fluxes are scaled using convective scaling parameters, namely the surface fluxes and the boundary layer heights from the LES data (Fig. 2, Table 2, and Fig. 4). The three vertical profiles at 1000, 1200, and 1400 CST from the homogeneous LES experiment are 15-min averages. As is evident in the figures, these LES results lie in between the observations.

The LES results reveal that the moisture fluxes decrease over time, whereas the buoyancy and CO_2 fluxes are closely clustered around a single curve. Grossman (1992), Davis et al. (1997), and LeMone et al. (2002) also found that the moisture exchange decreases during the daytime. This can be explained by the fact that in the morning, the ABL specific humidity decreases due to entrainment of dry air, which has a larger effect than the release of moisture at the surface. As a consequence, the jump at the inversion layer becomes smaller, resulting in smaller moisture entrainment under similar boundary layer growth conditions. At 1400 CST, the processes at the surface and at the inversion are in balance and the specific humidity remains constant at that time. This last remark is in agreement with Fig. 3 in which the two specific humidity profiles at 1152 and 1302 CST show similar boundary layer values. Near the entrainment region, negative buoyancy fluxes, positive specific humidity fluxes, and negative CO_2 fluxes are found, consistent with the signs of the jumps at the inversion layer in Fig. 3.

Entrainment is quantified and compared to the surface process by calculating the ratio (β_ψ) between the entrainment flux ($\overline{w'\psi'_e}$) and the surface flux ($\overline{w'\psi'_0}$) for virtual potential temperature, specific humidity, and CO_2:

$$\beta_\psi = -\frac{\overline{w'\psi'e}}{\overline{w'\psi'_0}}. \tag{2}$$

Linear extrapolations of the flux measurements between 1100 and 1400 CST to the boundary layer height ($z/z_i = 1$) give the following values: $\beta_{\theta_v} \approx 0$, $\beta_q \approx -2.2$, and $\beta_{CO_2} \approx -0.54$. These obtained values show the importance of the entrainment flux for moisture and carbon dioxide during the late morning and early afternoon. Except for the virtual potential temperature, the β values from the LES model between 1000 and 1400 CST are quite similar to the aircraft values, with $\beta_{\theta_v} \approx 0.2$, β_q between -1 and -2.4, and $\beta_{CO_2} \approx -0.5$. The disagreement between the two β_{θ_v} values is not surprising given the uncertainties introduced by extrapolating the aircraft fluxes upward to z_i.

Estimates of β_{θ_v} based on aircraft measurements in similar conditions are similar to our LES value, but typically larger than the aircraft value. Observed estimates show large variations, ranging from 0.08 ± 0.12 in Davis et al. (1997) to -0.03–0.8 in Grossman (1992) and 0.6 in Vilà-Guerau de Arellano et al. (2004). While in our study, we focus on one particular day, Davis et al. (1997) calculated an average β_{θ_v} value from 19 days that consists of morning and afternoon flights during the Boreal Ecosystem–Atmosphere Study (BOREAS-94) campaign. They also mentioned that these values are very sensitive to the determination of the ABL depth.

Grossman (1992) studied 2 days of the First International Satellite Land Surface Climatology Project (ISLSCP) Field Experiment (FIFE-87), and by using the linear extrapolation method to the top of the ABL, they found -0.03 for the day with light winds (<3 m s^{-1}) and 0.19 for the windy day (8–10 m s^{-1}) at around 1100 CDT. Furthermore, Vilà-Guerau de Arellano et al. (2004) found 0.6 from their analysis of 1 day at 1300 UTC during the European Union's Regional Assessment and Monitoring of the Carbon Balance within Europe (RECAB-02) project, in which the aircraft tracks were flown repeatedly at three levels in the ABL. Compared to the previous studies, our obtained aircraft value, $\beta_{\theta_v} \approx 0$, is relatively small, but higher aircraft legs in the entrainment zone are missing in order to obtain a better estimation using this extrapolation method. Previous LES studies (vanZanten et al. 1999; Pino et al. 2003; Conzemius and Fedorovich 2006) show values varying between 0.15 and 0.4, with larger values associated with the contribution of shear to the entrainment flux. Notice that LES experiments are controlled idealized numerical experiments, which do not suffer from the statistical uncertainties associated with observational estimates of entrainment. However, the effects of mesoscale eddies are not accounted for in the LES simulations.

Not surprisingly, large variability is observed for β_q, though most people report negative values. Previous studies based on aircraft measurements even show $\beta_q < -1$. For example, Davis et al. (1997) found a mean value of -1.57 over the boreal forest during daytime from late May to mid-September, and Vilà-Guerau de Arellano et al. (2004) found a mean value of -1.6 over grassland in the morning on a summer day. These values indicate that the exchange at the inversion layer is larger than at the surface.

Under convective conditions, the growth of the boundary layer is defined by the entrainment velocity $dh/dt > 0$. Therefore, the ratio for CO_2 can be either positive or negative, depending on the CO_2 mixing ratio difference between the ABL and the free atmosphere. With $\beta_{CO_2} < 0$, these aircraft measurements indicate that the turbulent eddies entrain air, containing a higher CO_2 mixing ratio. To our knowledge, there has been one previous estimation of the magnitude and evolution of β_{CO_2} (Vilà-Guerau de Arellano et al. 2004). In that study, $\beta_{CO_2} = 2.9$ was estimated from the aircraft measurements at 1300 UTC (afternoon), which was high compared to the mixed-layer model results, initialized with similar conditions as the day under study. In the mixed-layer model, β_{CO_2} decreased from 2.5 at 0900 UTC to -0.2 at 1600 UTC. Therefore, there is still considerable uncertainty about this value, its change in time, and its dependence on variations of the free-atmosphere values and boundary layer growth. In addition, the CO_2 production and uptake vary significantly and depend on the kind of vegetation, the activity of the vegetation (NDVI), and its moisture availability.

As illustrated by the foregoing, entrainment ratios depend largely on the boundary layer growth (entrainment velocity), the quantity distribution below and above the ABL, and the surface conditions. By assuming a sharp discontinuity at the inversion layer (zero-order jump approach), we are able to infer an estimation of the entrainment flux from the boundary layer growth and the jump at the inversion layer from the available aircraft observations. This relation between the entrainment flux and boundary layer dynamics is as follows:

$$\overline{w'\psi'_e} = -w_e \Delta\psi, \tag{3}$$

in which w_e is the entrainment velocity and $\Delta\psi$ is the jump at the top of the boundary layer. In our observations, an estimation of the entrainment velocity is $w_e = \partial h/\partial t \approx 0.03$ m s^{-1} at 1200 CST, assuming no large-scale subsidence. Using w_e and the jumps obtained from the vertical aircraft soundings in Fig. 3 leads to the following entrainment ratios: $\beta_{\theta_v} \approx 0.23$, $\beta_q \approx -1.3$, and $\beta_{CO_2} \approx -0.6$. In spite of the assumption of a sharp discontinuity at the inversion layer, all values appear to be reasonable and comparable to the ones directly estimated from the aircraft measurements and the homogeneous LES experiment.

b. Horizontal variability

Figure 6 shows the horizontal variability of the mean potential temperature, moisture, CO_2, wind components, and wind direction averaged over the eight 70 m AGL legs (left panel) and averaged over the three 700 m AGL legs (right panel). Both figures distinctly show higher potential temperatures, lower specific humidity, and lower CO_2 mixing ratios at the western part of the track. The differences between the two parts ($\Delta\psi = \psi_W - \psi_E$) are significant: $\Delta\theta \approx 0.7$ K, $\Delta q \approx -1$ g kg^{-1}, and $\Delta CO_2 \approx -3$ ppm. The wind at 70 m is uniformly from the southeast with a speed of nearly 4 m s^{-1}. The wind at 700 m is mainly coming from the south. In our analysis, we assume that a similar amount of heat, moisture, and CO_2 is advected from the south over the west and east parts of the flight track.

Assuming horizontal surface flux heterogeneity as shown in Fig. 1 but using comparable values of the surface stations, a heterogeneous LES experiment was

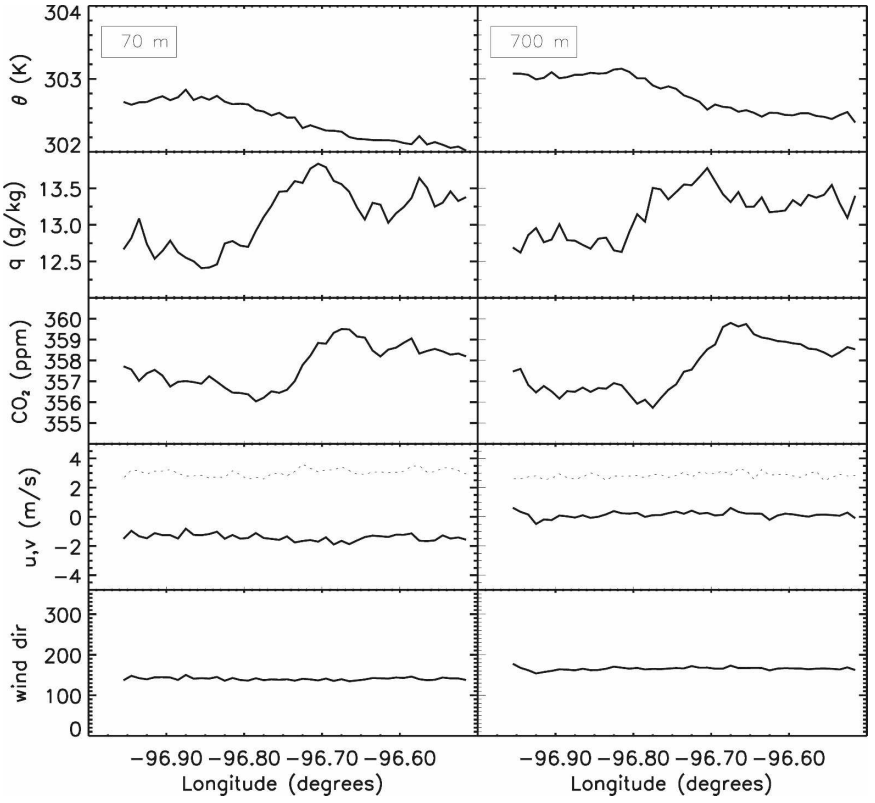

FIG. 6. Horizontal variability of (top to bottom) potential temperature, specific humidity, carbon dioxide mixing ratio, wind velocities, and wind direction averaged over (left) 8 legs at around 70 m and (right) 3 legs at around 700 m. The velocity u is the continuous line, and v is the dashed line.

performed prescribing a different surface flux amplitude (section 2) in order to determine to which height the surface heterogeneity influences the turbulent fluxes and how this relates to the boundary layer height. The imposed heterogeneity was designed to reflect the heterogeneity in Fig. 1 while keeping the fluxes close to those observed (Fig. 2), with H (LE) 20% higher (5% lower) than the homogeneous case over the western half of the domain, and H (LE) 20% lower (5% higher) than the homogeneous case over the eastern half of the domain. The quantities H + LE and CO_2 flux are the same for both halves of the domain.

Before analyzing the LES results and observations, it is interesting to quantify the impact of surface heterogeneity for the day under study by using a characteristic length scale. The minimum horizontal length scale of the surface heterogeneity that influences the flow through the whole ABL can be calculated by a scaling formulation suggested by Raupach and Finnigan (1995):

$$L_{\mathrm{Rau}} = C_{\mathrm{Rau}} \frac{U z_i}{w_*}, \tag{4}$$

in which $C_{\mathrm{Rau}} = 0.8$ is the nondimensional coefficient (Mahrt 2000), z_i is the ABL depth and $w_* = [(g z_i/\theta v)\overline{w\theta_s}]^{1/3}$ is the convective velocity scale, and U is normally the mean horizontal wind velocity. In our study, we have defined U as the wind component perpendicular to the direction of the surface heterogeneity changes. The estimated values from the observations at 1200 CST are $U \approx 1.7$ m s^{-1}, $z_i \approx 1100$ m, and $w_* \approx 1.5$ m s^{-1} such that a heterogeneity length scale of $L_{\mathrm{Rau}} \approx 1$ km is obtained for the day under study at 1200 CST for both observations and LESs. It is important to notice that the wind component U in the LES is entirely generated by the surface heterogeneity inducing a mesoscale circulation and depends on the heterogeneity length scale and the amplitude flux difference between both patches. As the heterogeneity length scale is 12.8 km in the heterogeneous LES experiment, which is larger than L_{Rau}, the turbulent fluxes and the boundary layer height should be influenced by the prescribed surface heterogeneity.

As an illustration of the LES simulation, we show a cross section of the potential temperature and horizontal and vertical wind velocity components from the

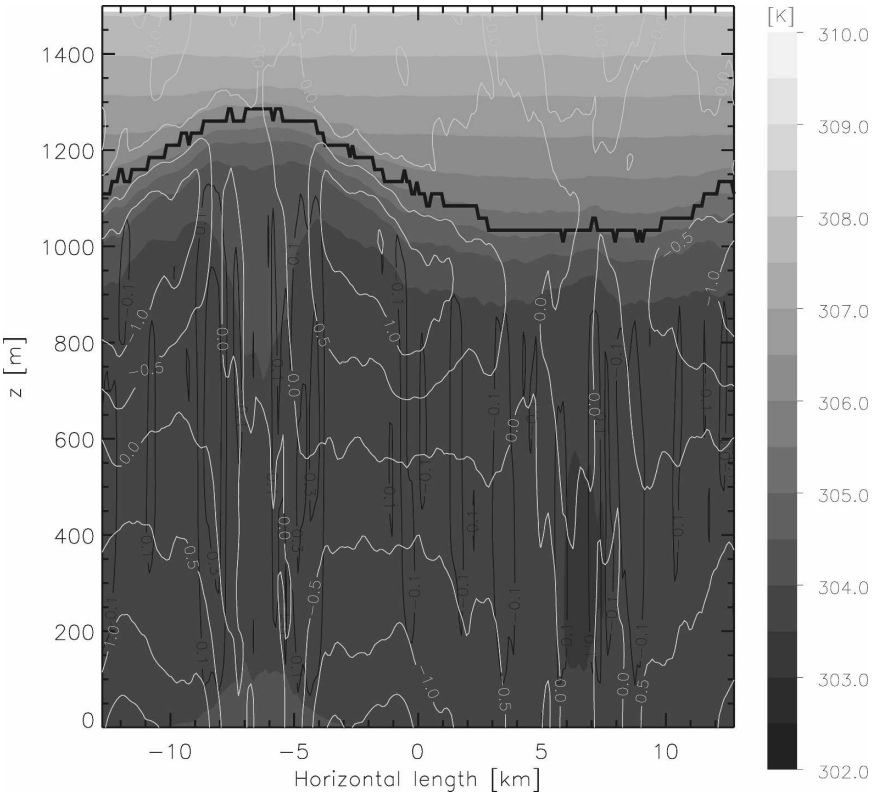

FIG. 7. Cross section of the potential temperature (shading), and vertical (thin black lines) and horizontal wind speeds (thin white lines) from the west–east direction for the heterogeneous LES experiment at 1200 CST, for a 15-min average. The thick black line represents the location of the boundary layer depth.

west–east direction for the heterogeneous LES experiment at 1200 CST, averaged over 15 min, in Fig. 7. The mixed-layer temperature is higher and the boundary layer is deeper over the west area than over the east area as a result of the larger sensible heat flux at the west. In addition, the air above the warm area in the west rises and the air above the cold area in the east descends. Consequently, near the surface cold and wet air is transported from the east to the west, and at the top of the boundary layer warm air is transported from the west to the east. In other words, a mesoscale circulation is originated. The maxima vertical wind velocities are 0.46 m s^{-1} upward, located above the west area, and 0.26 m s^{-1} downward, located above the east area. The observed minimum and maximum values of the horizontal wind speed are -1.8 m s^{-1} near the surface and 1.7 m s^{-1} near the entrainment zone, respectively.

Using the same procedure as in LeMone et al. (2003), we show in Fig. 8 the 4-km running means of the eight flight legs for NDVI and turbulent fluxes of sensible heat (H), latent heat (LE), and CO_2 ($\overline{w'CO_2'}$) at around 70 m AGL as a function of longitude from the observations and the heterogeneous LES experiment. The standard errors are calculated by $\sigma/n^{1/2}$, where $\sigma(i) = \sqrt{(1/8)\Sigma_{j=1}^{8}[F(i, j) - F_{ga}(i)]^2}$ is the temporal standard deviation and n is the number of legs. Here, $F(i, j)$ is the flux for each line segment i on the jth leg and $F_{ga}(i) = (1/8)\Sigma_{j=1}^{8}F(i, j)$ is the grand-average flux for each line segment centered at point i. There is not a clear difference between the fluxes at the east and west ends of the track, in contrast to the horizontal mean variations in Fig. 6. If we believe the measured fluxes, we are forced to conclude that the differences in the mean values result from a combination of horizontal differences in advection and entrainment. However, the fluxes at 70 m from the heterogeneous LES experiment show differences between the west and east parts. The LES fluxes are 1-km averages in which the distances in kilometers are replaced by 0.01° longitude starting at 96.87°W. The LES sensible heat flux at 70 m shows an east–west difference of approximately 40 W m^{-2}. The differences for LE are not so obvious. However, averaging LE for the eastern and western halves of the domain also produces a difference of 40 W m^{-2}. Following the same method as suggested by Patton et al. (2005), we notice that these fluxes calculated have been

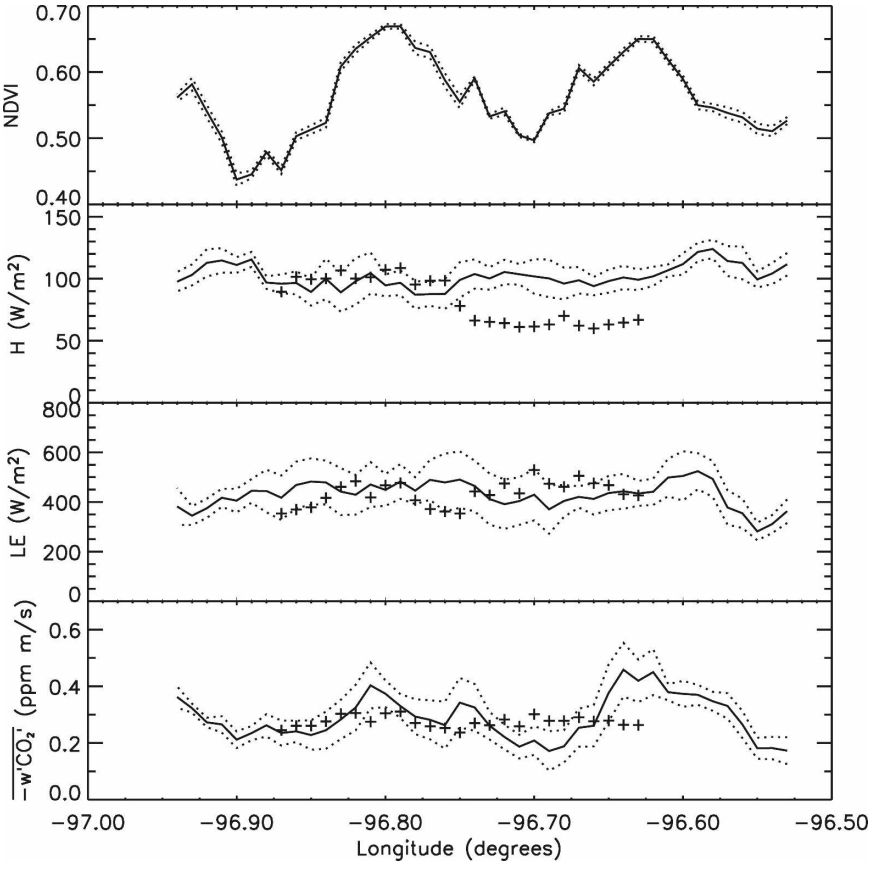

FIG. 8. The 4-km running means (over 8 legs) (continuous line) with their standard errors $[\sigma/(n)^{1/2}]$ (dotted line) for NDVI and for the turbulent fluxes of sensible heat (H), latent heat (LE), and carbon dioxide at around 70 m, calculated from the aircraft measurements between 1100 and 1400 CST. Plus signs are the fluxes at 70 m from the heterogeneous LES experiment from 96.65° to 96.85°W. Values for H (LE) are prescribed 20% higher (5% lower) in the western domain and 20% lower (5% higher) in the eastern domain than for the homogeneous case. Carbon dioxide fluxes are the same for both domains.

obtained by detrending and averaging over the north–south direction, characterized by uniform surface conditions. Larger differences between the fluxes as a function of longitude are expected if we detrend and average over the west–east direction, characterized by heterogeneous surface conditions. By using this procedure, the large fluctuations driven by the enhanced thermals above the west area become more pronounced.

Although the HRLDAS surface fluxes (Fig. 1), the 70-m fluxes from the heterogeneous LES experiment, and the measured thermodynamic variables along the flight track at 70 and 700 m AGL (Fig. 6) all show the effects of east–west surface heterogeneity, the calculated aircraft fluxes are more homogeneous (Fig. 8). A possible reason for these differences could be the overestimation of the surface heterogeneity by the HRLDAS model.

In Fig. 8 we also show the variations of NDVI along the flight track. There is a relationship between the fluxes and NDVI values, which vary between 0.4 and 0.7, but are not specifically higher at one end of the track. The NDVI maxima are located near 96.93°, 96.80°, and 96.62°W and the NDVI minima near 96.90°, 96.70°, and 96.55°W. High NDVI values correspond to green grass areas and low NDVI values correspond to areas of senescent winter wheat. As shown, CO_2 flux maxima (largest CO_2 uptake) are observed at the longitudes with high NDVI values. NDVI values show, indeed, a high correlation with the downward CO_2 fluxes (0.70), whereas the correlation values between NDVI and H or LE are relatively small (−0.34 and 0.32, respectively). However, it should be mentioned that the signs of the correlations are as expected. However, the correlation between H and LE is small (−0.07).

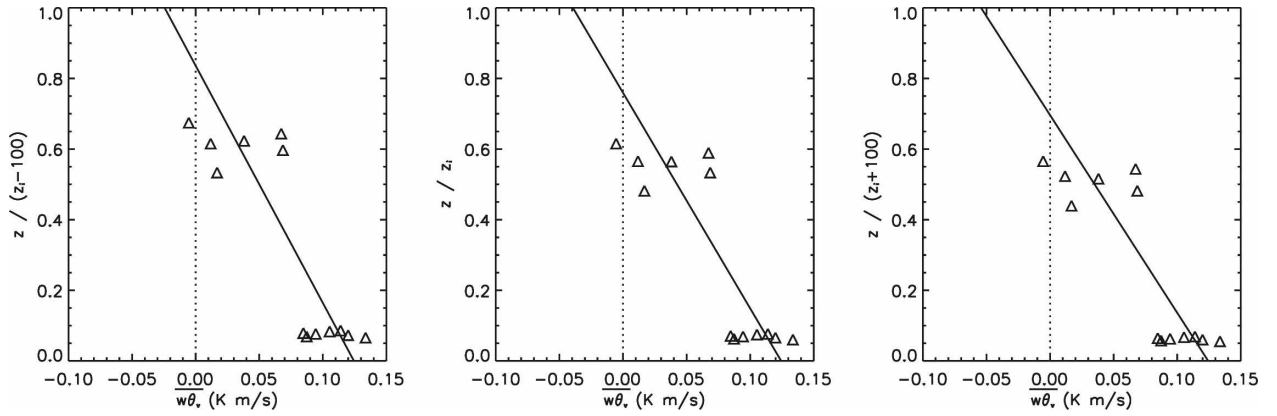

FIG. 9. Schematic representation of the least squares method to determine the surface and entrainment fluxes as a function of longitude calculated from the aircraft measurements for one 1-km segment of four-point running averages. To determine the scaling sensitivity of the boundary layer depth, scaling is applied with different boundary layer depths: (left) $z_i - 100$ m, (middle) z_i, and (right) $z_i + 100$ m, where z_i are the original ABL depth estimates from the homogeneous LES experiment at the specific leg times.

At 700 m AGL, the correlation between NDVI and the downward CO_2 fluxes is reduced to -0.18. Four possible reasons for this dropoff are 1) the influence of horizontal advection, 2) the effects of entrainment become more important at higher altitudes, 3) the surface area involved in the flux (footprint) changes with height, and 4) statistical uncertainty, with only 3 flight legs at 700 m represented in the average (in contrast to 8 flight legs at 70 m). Concerning CO_2 entrainment, this is not directly influenced by the CO_2 surface process as is the case for virtual potential temperature. In other words, there is no direct relationship between NDVI and CO_2 entrainment, because the CO_2 uptake at the surface is driven by the photosynthetic activity of the vegetation and entrainment is driven mostly by the surface heating.

Entrainment ratios ($\beta_\psi = -\overline{w'\psi'_e}/\overline{w'\psi'_0}$) were calculated for virtual potential temperature, specific humidity, and CO_2, for each 0.01° longitude (≈1 km) segment. To estimate these entrainment ratios, we need surface fluxes, the ABL top, and the fluxes at the ABL top. The ABL top is taken from the homogeneous LES experiment (Fig. 4). Although a spatial gradient in ABL depth of 100–200 m along the flight track was both observed on 30 May and simulated in the heterogeneous LES experiment (not shown), our first analysis is performed with a constant boundary layer height along the flight track. The aircraft fluxes used were four-point running averages of fluxes computed after linear detrending over the total leg as mentioned in section 2a.

A sample of a vertical virtual potential temperature flux profile is shown in Fig. 9 for one 1-km segment of four-point running averages for different boundary layer depth estimates: $z_i - 100$ m, z_i, and $z_i + 100$ m, where z_i are the original ABL depth estimates from the LES at the specific leg times. This is performed in order to determine the sensitivity of the entrainment ratio to the errors in the boundary layer depth estimates. These errors can be on the order of 100 m.

Figure 10 shows the obtained surface and entrainment fluxes for the virtual potential temperature, specific humidity, and carbon dioxide mixing ratio as a function of longitude from the vertically extrapolated aircraft measurements. The surface fluxes show patterns similar those for the fluxes at 70 m (Fig. 8). Maxima for all three entrainment fluxes are observed at approximately 96.80° and 96.53°W and minima at approximately 96.57° and 96.90°W. As the three entrainment fluxes are all related to the entrainment velocity, it is not surprising that there are reasonable correlation values among the three entrainment fluxes (between 0.51 and 0.64).

The entrainment ratios based on Fig. 10 are shown as a function of longitude in Fig. 11. This figure is a very qualitative picture and only provides information on the possible variation of this ratio, due to the uncertainties associated with the high-altitude legs. However, the mean values over the track, $\beta_{\theta_v} \approx 0.10$, $\beta_q \approx -2.4$, and $\beta_{CO_2} \approx -0.58$, are similar to the values found with the observations using the single-value method and values found from the homogeneous LES experiment. Higher boundary layer height estimates ($z_i + 100$ m) lead to larger entrainment flux estimates and, consequently, to a higher mean entrainment ratio ($\beta_{\theta_v} \approx 0.20$).

In general, the entrainment flux consists of two components: 1) entrainment driven by mesoscale fluctuations generated by the thermal differences $(\overline{w\theta_v})_e$, and 2) entrainment at smaller scales, related to the imping-

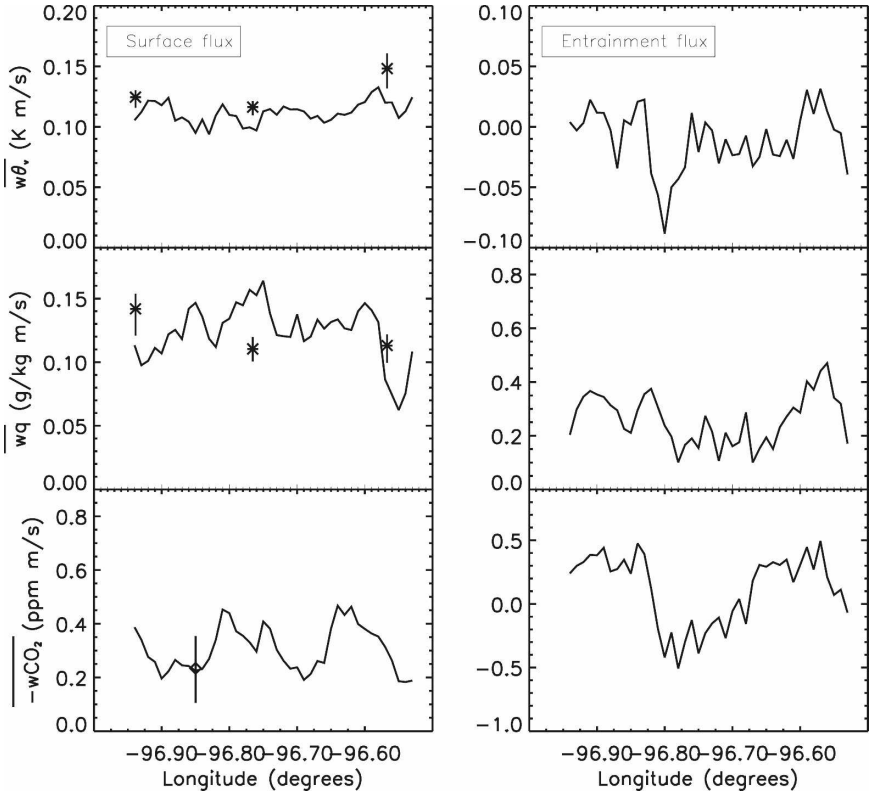

FIG. 10. (left) Surface and (right) entrainment fluxes for (top) virtual potential temperature, (middle) specific humidity, and (bottom) carbon dioxide mixing ratio as a function of longitude, calculated from the aircraft measurements between 1100 and 1400 CST. Both values have been extrapolated from the aircraft measurements. Symbols are the mean surface fluxes of the three surface stations (sensible and latent heat are represented by an asterisk in top-left and middle-left panels) and the Smileyberg site (carbon dioxide is represented by a circle in the bottom panel) and their minimum and maximum values between 1100 and 1400 CST.

ing of eddies at the inversion zone $(\overline{w'\theta_v'})_e$ (Patton et al. 2005; van Heerwaarden and Vilà-Guerau de Arellano 2008). The first process could contribute to the second. In our case, we have chosen to study the second process; the first one is still an open issue. Regarding β_{θ_v}, it varies between −0.3 and 0.8. Larger values at certain longitudes can occur despite the fact that the surface is rather homogeneous.

As for β_q, it is always negative and varies between −7 and −0.5. As discussed in the previous section, this range of values has also been observed in other studies. The BL will become drier as long as the entrainment of dry air from the free atmosphere is larger than the moisture release at the surface.

The entrainment ratio β_{CO_2} ranges between −2 and 1.5. A few positive ratios are observed and indicate positive entrainment fluxes, which can only occur when the CO_2 concentration is higher in the boundary layer than in the free atmosphere or the positive values could be a side effect of extrapolation in the presence of statistical uncertainty. In general, the entrainment ratios of specific humidity and carbon dioxide can vary significantly due to their dependence on boundary layer dynamics, surface conditions, and variations in the conditions of the boundary layer and the free atmosphere. Low correlation values are observed between NDVI and the three entrainment ratios. This is not surprising, because low correlation values were already found between NDVI and H (or LE) at 70 m AGL and the correlation was reduced between NDVI and the CO_2 fluxes at 700 m AGL.

4. Conclusions

The horizontal variability of virtual potential temperature, moisture, and carbon dioxide fluxes in the boundary layer is studied by analyzing aircraft measurements in southeast Kansas on 30 May 2002 from the IHOP_2002 project. On this day, characterized by clear skies and south-to-southeast winds of about 4 m s^{-1}, the development of the boundary layer was

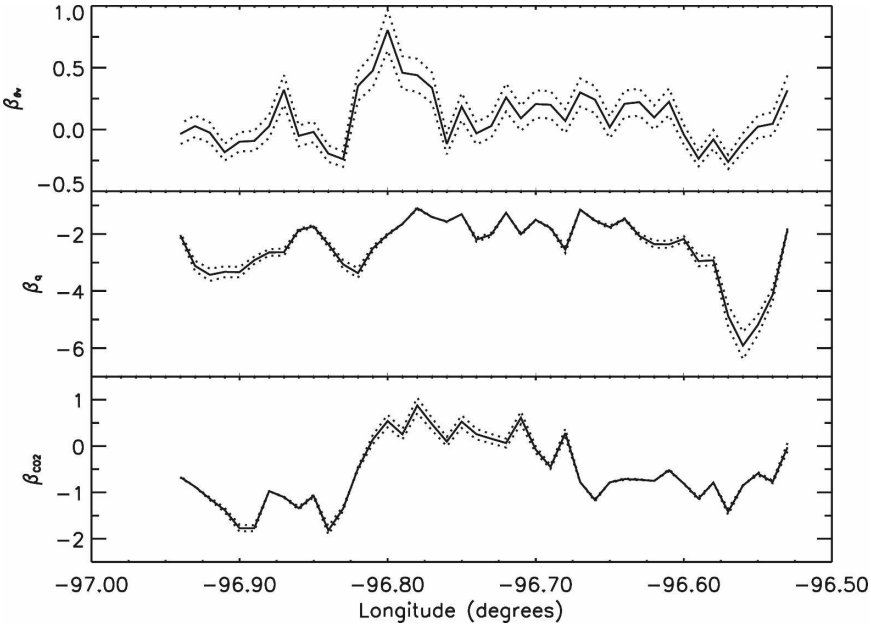

FIG. 11. The entrainment ratios β for (top) virtual potential temperature, (middle) specific humidity, and (bottom) carbon dioxide mixing ratio as a function of longitude, calculated from the aircraft measurements between 1100 and 1400 CST (solid line) and the ratios from calculations with $z_i \pm 100$ m (dotted lines).

mainly driven by convective turbulence. Under the meteorological conditions of 30 May, the relationship between horizontal variations of mean and flux values and surface heterogeneity is discussed, with emphasis on the vertical structure and the horizontal variability of the turbulent fluxes in relation to land-use characteristics.

Measurements gathered during several horizontal aircraft passages reveal two regions, characterized by warm and dry conditions (western part) and cold and wet conditions (eastern part). These differences in ABL thermodynamics are consistent with the east–west trends in the surface sensible and latent heat fluxes from HRLDAS simulations. However, the fluxes at 70 m calculated from the aircraft measurements do not exhibit the east–west trends that the HRLDAS model predicts.

A large-eddy simulation model was used to complement the observational study and to obtain additional information on the temporal evolution of the boundary layer dynamics of the day under study. A homogeneous numerical experiment was carried out by prescribing similar initial and surface conditions as were observed during 30 May 2002. In the homogeneous LES experiment, the fluxes and boundary layer depth evolution are consistent with the observations.

Assuming first the surface to be homogeneous and working with aircraft leg averages, we estimated the turbulent fluxes as a function of height. Based on these profiles and boundary layer depths from the LES, we calculated the negative of the ratio of the entrainment flux and the surface flux between 1100 and 1400 CST for virtual potential temperature, $\beta_{\theta_v} \approx 0$; for specific humidity, $\beta_q \approx -2.2$; and for carbon dioxide, $\beta_{CO_2} \approx -0.54$. The entrainment ratios obtained from the LES model are quite similar to the ratios from the aircraft measurements, except for the buoyancy ratio, $\beta_{\theta_v} \approx 0.2$. Furthermore, the entrainment ratios remain constant in time for virtual potential temperature and CO_2 between 1000 and 1400 CST, but a decrease is observed for moisture, as observed in earlier studies.

Based on NDVI estimates from aircraft measurements along a nearly east–west track and the strong east–west differences in the HRLDAS simulations of the sensible and latent heat fluxes, the surface should be rather heterogeneous. Therefore, we estimated the means and turbulent fluxes as a function of longitude, following LeMone et al. (2007a). Although a clear distinction in the means between the west and east parts is observed, the turbulent fluxes do not have a strong east–west trend. The sensible and latent heat fluxes are loosely related to NDVI values, which represent the photosynthetic activity and are therefore a measure of the variability in surface properties. However, these NDVI values show a high correlation with the CO_2 fluxes at 70 m (0.70), whereas the correlation is reduced

higher in the BL at 700 m (−0.18). This can be explained by the greater importance of entrainment at higher altitudes, the surface area involved in the flux (footprint) changing with height, and the smaller sample (three legs) at 700 m causing higher statistical uncertainty.

The heterogeneous LES experiment, carried out to estimate the horizontal distribution of the fluxes above the surface using surface fluxes heterogeneity similar to those predicted in HRLDAS, showed horizontal variability at the same scales that were strong for H and weaker for LE. That this did not appear in the observations suggests to us that HRLDAS exaggerated the east–west gradient in the fluxes for this day. In addition, HRLDAS failed to replicate the horizontal variability associated with NDVI, a shortcoming probably related to the fact that most of the land use along the flight track was characterized as grassland even though LeMone et al. (2007a) show a strong association of NDVI variation with winter wheat.

A first attempt is made to estimate the horizontal variability of the entrainment ratios as a function of the longitude, although this field campaign was not specially assigned for a study on entrainment at the interface. Robust estimates will require a more specific aircraft measurement strategy. Horizontal variability of the entrainment ratios is shown for each variable, but specific humidity and CO_2 show larger scatter than does the virtual potential temperature. This might be explained by the fact that the moisture and CO_2 processes at the surface and at the top of the BL are not dynamically coupled processes and depend on boundary layer dynamics and the distribution of moisture and CO_2 below and above the ABL. The methodology presented here, and based on the determination of the horizontal variability of fluxes from observations and controlled numerical experiments, show a great potential for determining the coupling between the boundary layer dynamics and the atmospheric flow influenced by surface flux differences.

Acknowledgments. This research is supported by the Wageningen Institute for Environment and Climate Research (WIMEK). The large-eddy simulations were done at SARA under a National Computer Faculty contract (NCF SG-06-132). Funding for the visit at the National Center for Atmospheric Research in Boulder was provided by the Netherlands Organization for Scientific Research (R76-262).

REFERENCES

Avissar, R., and T. Schmidt, 1998: An evaluation of the scale at which ground-surface heat patchiness affects the convective boundary layer using large-eddy simulations. *J. Atmos. Sci.,* **55,** 2666–2689.

Chen, F., and Coauthors, 2007: Evaluation of the characteristics of the NCAR High-Resolution Land Data Assimilation System. *J. Appl. Meteor. Climatol.,* **46,** 694–713.

Conzemius, R. J., and E. Fedorovich, 2006: Dynamics of sheared convective boundary layer entrainment. Part I: Methodological background and large eddy simulations. *J. Atmos. Sci.,* **63,** 1151–1178.

Coulter, R. L., M. S. Pekour, D. R. Cook, G. E. Klazura, T. J. Martin, and J. D. Lucas, 2006: Surface energy and carbon dioxide fluxes above different vegetation types within able. *Agric. For. Meteor.,* **136,** 147–158.

Cuijpers, J. W. M., and P. G. Duynkerke, 1993: Large eddy simulations of trade wind with cumulus clouds. *J. Atmos. Sci.,* **50,** 3894–3908.

Davis, K. J., D. H. Lenschow, S. P. Oncley, C. Kiemle, G. Ehret, A. Giez, and J. Mann, 1997: Role of entrainment in surface–atmosphere interactions over the boreal forest. *J. Geophys. Res.,* **102,** 29 219–29 230.

Deardorff, J. W., 1980: Stratocumulus-capped mixed layers derived from a three-dimensional model. *Bound.-Layer Meteor.,* **18,** 495–527.

Desjardins, R. L., R. L. Hart, J. I. MacPherson, P. H. Schuepp, and S. B. Verma, 1992: Aircraft- and tower-based fluxes of carbon dioxide, latent, and sensible heat flux. *J. Geophys. Res.,* **97,** 18 477–18 485.

Dosio, A., J. Vila-Guerau de Arellano, A. A. M. Holtslag, and P. J. H. Builtjes, 2003: Dispersion of a passive tracer in buoyancy- and shear-driven boundary layers. *J. Appl. Meteor.,* **42,** 1116–1130.

Gerbig, C., J. C. Lin, S. C. Wofsy, B. C. Daube, A. Andrews, B. B. Stephens, P. S. Bakwin, and C. A. Grainger, 2003: Toward constraining regional-scale fluxes of CO_2 with atmospheric observations over a continent: 1. Observed spatial variability from airborne platforms. *J. Geophys. Res.,* **108,** 4756, doi:10.1029/2002JD003018.

Grossman, R. L., 1992: Convective boundary layer budgets of moisture and sensible heat over an unstressed prairie. *J. Geophys. Res.,* **97,** 18 425–18 438.

Kang, S., K. J. Davis, and M. A. LeMone, 2007: Observations of the ABL structures over a heterogeneous land surface during IHOP_2002. *J. Hydrometeor.,* **8,** 221–244.

Kim, J., and S. B. Verma, 1990: Carbon dioxide exchange in a temperate grassland ecosystem. *Bound.-Layer Meteor.,* **52,** 135–149.

LeMone, M. A., and Coauthors, 2002: CASES-97: Late-morning warming and moistening of the convective boundary layer over the Walnut River watershed. *Bound.-Layer Meteor.,* **104,** 1–52.

——, R. L. Grossman, F. Chen, K. Ikeda, and D. Yates, 2003: Choosing the averaging interval for comparison of observed and modeled fluxes along aircraft transects over a heterogeneous surface. *J. Hydrometeor.,* **4,** 179–195.

——, and Coauthors, 2007a: NCAR/CU surface, soil, and vegetation observation network during the IHOP2002 field campaign. *Bull. Amer. Meteor. Soc.,* **88,** 65–81.

——, F. Chen, J. G. Alfieri, M. Tewari, B. Geerts, Q. Miao, R. L. Grossman, and R. L. Coulter, 2007b: Influence of land cover, soil moisture, and terrain on the horizontal distribution of sensible and latent heat fluxes and boundary layer structure in southeast Kansas during IHOP2002 and CASES-97. *J. Hydrometeor.,* **8,** 68–87.

Lloyd, J., and J. A. Taylor, 1994: On the temperature dependence of soil respiration. *Functional Ecol.,* **8,** 315–323.

Mahrt, L., 2000: Surface heterogeneity and vertical structure of the boundary layer. *Bound.-Layer Meteor.,* **96,** 33–62.

——, J. I. MacPherson, and R. Desjardins, 1994: Observations of fluxes over heterogeneous surfaces. *Bound.-Layer Meteor.,* **67,** 345–367.

Patton, E. G., P. P. Sullivan, and C.-H. Moeng, 2005: The influence of idealized heterogeneity on wet and dry planetary boundary layers coupled to the land surface. *J. Atmos. Sci.,* **62,** 2078–2097.

Pino, D., J. Vilà-Guerau de Arellano, and P. G. Duynkerke, 2003: The contribution of shear to the evolution of a convective boundary layer. *J. Atmos. Sci.,* **60,** 1913–1926.

Raupach, M. R., and J. J. Finnigan, 1995: Scale issues in boundary-layer meteorology: Surface energy balances in heterogeneous terrain. *Hydrol. Processes,* **9,** 589–612.

Siebesma, A. P., and J. W. M. Cuijpers, 1995: Evaluation of parametric assumptions for shallow cumulus convection. *J. Atmos. Sci.,* **52,** 650–666.

Strunin, M. A., and T. Hiyama, 2005: Spectral structure of small-scale turbulent and mesoscale fluxes in the atmospheric boundary layer over a thermally inhomogeneous land surface. *Bound.-Layer Meteor.,* **117,** 479–510.

Sullivan, P. P., C.-H. Moeng, B. Stevens, D. H. Lenschow, and S. D. Mayor, 1998: Structure of the entrainment zone capping the convective atmospheric boundary layer. *J. Atmos. Sci.,* **55,** 3042–3064.

van Heerwaarden, C. C., and J. Vilà-Guerau de Arellano, 2008: Relative humidity as an indicator for cloud formation over heterogeneous land surfaces. *J. Atmos. Sci.,* **65,** 3263–3277.

vanZanten, M. C., P. G. Duynkerke, and J. W. M. Cuijpers, 1999: Entrainment parameterization in convective boundary layers derived from large eddy simulations. *J. Atmos. Sci.,* **56,** 813–828.

Verma, S. B., J. Kim, and R. J. Clement, 1989: Carbon dioxide, water vapor and sensible heat fluxes over a tallgrass prairie. *Bound.-Layer Meteor.,* **46,** 53–67.

Vilà-Guerau de Arellano, J., B. Gioli, F. Miglietta, H. J. J. Jonker, H. K. Baltink, R. W. A. Hutjes, and A. A. M. Holtslag, 2004: The entrainment process of carbon dioxide in the atmospheric boundary layer. *J. Geophys. Res.,* **109,** 18 110–18 124.

Weckwerth, T., and Coauthors, 2004: An overview of the International H_2O Project (IHOP2002) and some preliminary highlights. *Bull. Amer. Meteor. Soc.,* **85,** 253–277.

Wicker, L. J., and W. C. Skamarock, 2002: Time-splitting methods for elastic models using forward time schemes. *Mon. Wea. Rev.,* **130,** 2088–2097.

Yi, C., K. J. Davis, P. S. Bakwin, A. S. Denning, N. Zhang, A. Desai, J. C. Lin, and C. Gerbig, 2004: Observed covariance between ecosystem carbon exchange and atmospheric boundary layer dynamics at a site in northern Wisconsin. *J. Geophys. Res.,* **109,** D08302, doi:10.1029/2003JD004164.